

# Parallel electric fields produced by the ionospheric injection

Office Geophysik, Ogoori, 838-0141, Japan

Osuke Saka

saka.o@nifty.com

## Abstract

It is well known that there exists a thin layer in the lower boundary of the ionosphere between altitudes of 80 km and 140 km in which collisional ions and collisionless electrons mix. Local breakdown of charge neutrality may be initiated in this layer by electric fields from the magnetosphere as well as by electric fields generated there by the local neutral winds. The breakdown may be momentarily canceled by the Pedersen currents, but a complete neutralization is prevented because some ionospheric plasmas are released as outflows by parallel electric fields. Those parallel electric fields are produced by inherent plasma processes in the polar ionosphere and act as auroral drivers. New scenario creating parallel potential gradients is proposed.

## 1. Introduction

The Poynting flux of the fields and particle momentum carried by double layer or electrostatic shock generate parallel electric fields in the magnetosphere [Block, 1977; Goertz and Boswell, 1979]. Field-aligned plasma flows in converging field geometry are mechanical energies that excite parallel electric fields by the charge separations along the field lines due to the magnetic mirroring of electrons and ions [Sato, 1982; Schriver and Ashour-Abdalla, 1993]. Open fields interacting with the solar wind and a charge separation across the nightside magnetosphere due to the plasma convections in the magnetosphere create parallel electric fields [Lyons, 1980; Stern, 1981]. These parallel potentials associated with the magnetospheric generators are used to infer FAC in the magnetosphere [Knight, 1973; Chiu and Schulz, 1978].

The ionosphere as generator has the capability to produce electrostatic potential itself, once the electric fields are transmitted along field lines into the auroral zone from the magnetosphere or produced there by the local neutral winds [Saka, 2021b]. While these electric fields that have penetrated the E region may accumulate collisionless electrons at a leading edge of flow channels caused by the ExB drift, collisional ions cannot follow them.

37 The negative potential thus produced at the leading edge of flow channels in the E region  
38 generates upward electric fields as an auroral driver. Although this conjunction is inconsistent  
39 with Gauss's theorem, it can be understood if a positive space charge was generated  
40 immediately above the ionosphere. The above description is consistent with the formation of  
41 an incomplete Cowling channel [Baumjohann, 1980], except that upward field-aligned  
42 currents are created at the negatively charged southern border [Saka, 2021b].

43 Ionospheric potential may be observed in the global current circuit of the ionosphere-  
44 atmosphere-earth system. The currents in this circuit are generated in the atmosphere by  
45 charge separation processes in tropical convective storms. The current influenced by the  
46 ionospheric potential can be detected in this global circuit by monitoring vertical component  
47 ( $B_z$ ) of the ground magnetometer data. Reduction of  $B_z$  on the ground correlates with  
48 decrease of atmospheric electric field on the ground [Minamoto and Kadokura, 2011]. Such  
49 correlation would occur in connection with the potential drop of the ionosphere above the  
50 ground station [Saka, 2021a].

51 The proposed new scenario referred to as ionospheric injection is summarized in Sect.  
52 2. Summary and discussion are presented In Sect. 3.

53

## 54 *2. Ionospheric injection*

55 Distribution of the pitch angle along the field lines can be expressed using constant of  
56 the motion,

$$57 \quad \mu = \frac{m_q}{2B} v^2 \sin^2 \alpha \quad (1)$$

58 Here,  $\alpha$  denotes pitch angle at the magnetic field  $B$ , and  $m_q v^2 / 2$  is kinetic energy of  
59 particle  $q$ . Substituting  $B_R$  at the mirror height ( $\sin^2 \alpha = 1$ ), altitude profiles of the pitch  
60 angle in the absence of the parallel electric fields can be given as,

$$61 \quad \sin^2 \alpha = \frac{B}{B_R} \quad (2)$$

62 Figure 1 shows altitude profile of  $\sin^2 \alpha$  along  $L=6$  of the dipole fields from the ionosphere  
63 (100 km) to 10,520 km above it.

64 Pitch angle curve along the field lines shown in Figure 1 could be modified by the  
65 presence of the parallel electric fields. Two types of the parallel electric fields are discussed,  
66 one being transient and the other steady-state. Direction of the transient electric field is  
67 downward into the ionosphere and that of the steady-state electric field is upward out of the  
68 ionosphere (Figure 2).

69

70 *2.1 Excitation of transient electric fields*

71 We assume negative potential regions are produced by the local breakdown of the charge  
72 neutrality. This breakdown occurred in a thin layer located at boundaries between  
73 mesosphere and thermosphere where collisional ions and collisionless electrons mix  
74 [Rishbeth and Garriot, 1969]. The thin layer extends between altitude of 80 km to 140 km  
75 and is hereafter referred to as the ionosphere.

76 We assume that the negative charge sheet (1280km in longitudes and 128km in  
77 latitudes) was developed in the ionosphere. The thickness of the sheet is assumed to be  
78 equivalent to the same 60km thickness of the ionosphere. Emerged charge density is  
79 assumed to be  $5 \times 10^2 m^{-3}$  in the sheet. Vertical electric fields generated by the negative  
80 charge sheet are directed down into the ionosphere (Figure 2). Altitude profiles of the  
81 downward electric fields through the center of the sheet are colored red in Figure 3-1. For  
82 comparison, magnetic mirror force in mV/m is presented in black, assuming  $\mu = 0.16 eV / nT$ ,

83 corresponding to  $\frac{mv_{\perp}^2}{2} = 1keV$  at  $X=1Re$  (6240nT). Force arising from electrostatic fields

84 exceeds the magnetic mirror force below 3,643km in altitudes. When the spatial scale of the  
85 negative charge sheet decreased to 640km x 64km, the crossover altitudes of two forces  
86 decreased to 1,830km (Figure 4-1).

87 Downward electric fields change pitch-angle trajectories of electrons approaching the  
88 ionosphere from the magnetosphere by decelerating the parallel velocities. Mirror height  
89 moved to 1,407km (Figure 3-2). For the smaller scale charge sheet, new mirror height is  
90 590km (Figure 4-2). For purposes of reference, pitch-angle trajectories in the absence of the  
91 parallel electric fields ( $\sin^2 \alpha$  vs  $X$ ) are plotted in black. Pitch-angle trajectories of electrons  
92 bend clockwise with new mirror height. These are shown in Figure 3-2 and Figure 4-2 in red.  
93 Ions may not change pitch-angle trajectories in a bounce time of electrons (few seconds)  
94 because of the mass ratio.

95 As a result, there appeared three regions designated as A, B, C in the pitch-angle plane  
96 (Figure 3-2 and Figure 4-2). In (A), electrons and ions are in loss cone, in (B), ions are trapped  
97 but electrons from loss cone decelerated by downward electric fields filled this region due to  
98 magnetic mirroring, and in (C), electrons and ions are trapped. Pitch-angle discrepancy  
99 appears only in region (B): electrons are loss cone populations while ions are trapped  
100 populations.

101 According to Persson (1963), the number densities of hot plasmas are calculated  
102 substituting isotropic Maxwellian distribution of temperature  $T_q$ ,

103  $f_{trap}(v_{//}, v_{\perp}) = \left( \frac{m_q}{2\pi k T_q} \right)^{3/2} \exp\left( -\frac{m_q}{2k T_q} (v_{//}^2 + v_{\perp}^2) \right)$  out of the loss cone, and

104  $f_{loss}(v_{//}, v_{\perp}) = c f_{trap}(v_{//}, v_{\perp})$  in the loss cone

105 into

$$106 \quad \frac{n_q}{n_0} = 2\pi \int [f_{trap}(v_{//}, v_{\perp}) + f_{loss}(v_{//}, v_{\perp})] v_{\perp} dv_{\perp} dv_{//} \quad (3)$$

107 Here, q is applicable to either electrons or ions. We assume that loss cone particles are  
 108 removed from the flux tubes and are empty ( $c = 0$ ) prior to the auroral evolutions arising out  
 109 of the onset arc, or before the following auroral onset.

110 Normalized density difference,  $(n_i - n_e)/n_0$ , before the auroral onset ( $c = 0$ ) is shown  
 111 in Figure 3-3 (Figure 4-3). When we choose  $c = 0.5$ , normalized density difference shown  
 112 in Figure 3-3 (Figure 4-3) was reduced by half. Positive charges emerged immediately above  
 113 the ionosphere. The excess electrons repelled from both hemispheres due to magnetic  
 114 mirroring would create the electron rich regions in the magnetosphere.

115

## 116 2.2 Steady-state solution of parallel electric fields

117 In the one-dimensional model, parallel electric fields at  $s_1$  are calculated by  
 118 integrating the density difference along field lines  $s$ ,

$$119 \quad E_{//}(s_1) = \int_{s_0}^{s_1} \frac{e(n_i - n_e)}{\epsilon_0} ds \quad (4)$$

120 Here  $s_0$  denotes ionospheric altitude where integration starts.

121 These are plotted in Figure 3-4 (Figure 4-4) starting from the ionosphere (0 km) to a  
 122 point 10,520 km. At this altitude, the upward electric fields are not vanished, because electron  
 123 rich region may be located far up in the magnetosphere. To plot profiles of the parallel electric  
 124 fields, geometrical factor ( $\sqrt{B_{s_1}/B_{s_0}}$ ) was multiplied to  $E_{//}(s_1)$  for adjusting the diverging  
 125 geometry of the dipole configuration.  $E_{//}(s_1)$  is linearly proportional to the background hot  
 126 plasma density supplied from the tail. In this plot, hot plasma density  $n_0 = 10^{-1} m^{-3}$  was  
 127 assumed.

128 These parallel electric fields are generated by charge separations along the diverging  
 129 magnetic fields, with positive charges immediately above the ionosphere and negative  
 130 charges in the magnetosphere constituting steady-state solutions of the flux tubes [Alfven  
 131 and Falthammar, 1963; Persson, 1966]. Generation of upward electric fields above the

132 negative charge sheet resembles battery connected in series to the negative electrode in the  
133 ionosphere. Transient electric fields of opposite polarity would be shielded by the space  
134 charge built up along the field line. The lifetime of the transient electric fields is few seconds,  
135 a time required for building up the space charge or bounce time of electrons. Steady-state  
136 electric fields may persist until charge separation along field lines is neutralized. Because  
137 flux tube contains parallel electric fields pointing upward, neutralization may occur locally and  
138 intermittently accompanying auroral precipitation. We assume that loss cone electrons are  
139 removed by the downward acceleration before the start of following auroral evolutions.

140

### 141 *3. Summary and Discussion*

142 Vertical electric fields develop transiently in the ionosphere and produce different angular  
143 distributions of ions and electrons in the magnetosphere. These transients yield charge  
144 separations along the field lines. Charge separations along the field lines produce steady-  
145 state parallel electric fields in the magnetosphere.

146 The transients are usually triggered by the transverse electric fields transmitted from  
147 the magnetosphere during the dipolarization onset. We also consider the cases where  
148 breakdown of the charge neutrality was initiated in the polar ionosphere by the neutral winds.  
149 Neutral wind generates positive charge in the leading edge of wind channel and negative  
150 charge in the trailing edge; the ExB drift (E is polarization electric fields in the wind channel)  
151 generates negative charge to one side and positive to the other side of the wind channel.  
152 Auroras are produced in the negative charge region. If wind velocity is weaker than ExB drift,  
153 breakdown of the charge neutrality may not happen because polarization drift of ions  
154 suppressed the charging up of the ionosphere. Wind velocities of the order of  $10^3 m/s$  are  
155 necessary to produce substorm auroras by the neutral wind. This scenario may be  
156 reminiscent of auroras among gas planets in the solar system such as weather-driven  
157 auroras in Saturn [Chowdhury et al., 2021].

158

159

160

161

### 162 *4. Data availability*

163 No data sets were used in this article.

164

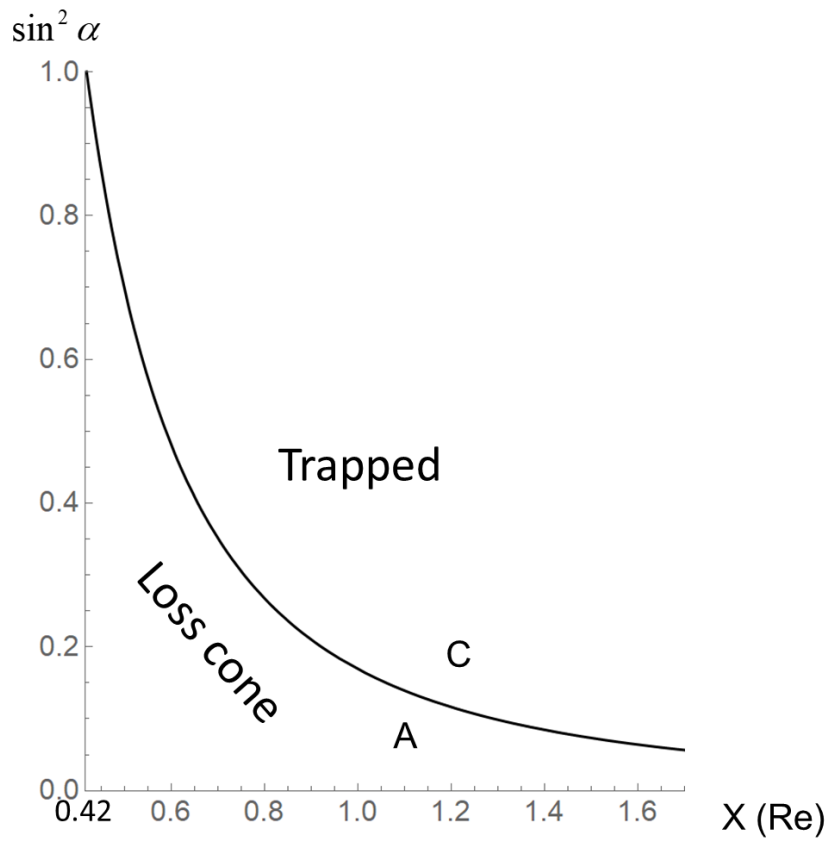
165

### 166 *5. Competing interest*

167 The author declares that there is no conflict of interest.

168  
169  
170  
171  
172 References  
173 Alfvén, H. and Fälthammar, C.-G.: *Cosmical Electrodynamics*, 2<sup>nd</sup> Edn., Oxford University  
174 Press, New York, 1963.  
175 Baumjohann, W.: Ionospheric and field-aligned current systems in the auroral zone: a  
176 concise review, *Adv. Space Res.*, 2, 55-62, 1983.  
177 Block, L.P.: Double layer review, Tech. Rep. TRITA-EPP-77-16, Dep. Plasma Phys., Roy.  
178 Insti. of Technol., Stockholm, Sweden, 1977.  
179 Chiu, Y.T., and Schulz, M.: Self-consistent particle and parallel electrostatic field  
180 distributions in the Magnetospheric-Ionospheric auroral region, *J. Geophys. Res.*, 83,  
181 629-642, 1978.  
182 Chowdhury, N.M., Stallard, T.S., Baines, K.H., Provan, G., Melin, H., Hunt, J.G., Moore, L.,  
183 O'Donoghue, J., Thomas, E.M., Wang, R., Miller, S., and Badman, S.V.: Saturn's  
184 weather-driven aurorae modulate oscillations in the magnetic field and radio  
185 emissions, *Geophys. Res., Lett.*, 49, e2021GL096492, 2021.  
186 Goertz, C.K., and Boswell, R.W.: Magnetosphere-Ionosphere coupling, *J. Geophys. Res.*,  
187 84, 7239-7246, 1979.  
188 Knight, S.: Parallel electric fields, *Planet. Space Sci.*, 21, 741-750, 1973.  
189 Lyons, L.R.: Generation of large-scale regions of auroral currents, electric potentials, and  
190 precipitation by the divergence of the convection electric field, *J. Geophys. Res.*, 85,  
191 17-24, 1980.  
192 Minamoto, Y., and Kadokura, A.: Extracting fair-weather data from atmospheric electric-  
193 field observations at Syowa Station, Antarctica, *Polar Sci.*, 5, 313-318, 2011.  
194 Persson, H.: Electric field along a magnetic line of force in a low-density plasma, *Physics*  
195 *Fluids*, 6, 1756-1759, 1963.  
196 Persson, H.: Electric field parallel to the magnetic field in a low-density plasma, *Physics*  
197 *Fluids*, 9, 1090-1098, 1966.  
198 Rishbeth, H., and Garriott, O.K.: *Introduction to ionospheric physics*, *International*  
199 *Geophysics*, 14, 1-331, 1969.  
200 Saka, O., Effects of auroral Ionosphere on atmospheric electricity, PEM11-P06, Abstract  
201 presented in JpGU2021,2021a.  
202 Saka, O.: Ionospheric control of space weather, *Ann. Geophys.* 39, 455-460, 2021b.

- 203 Sato, T.: Auroral physics, Magnetospheric plasma physics Ed Nishida, D.Reidel Pub. Com.,  
204 1982.
- 205 Schriver, D., and Ashour-Abdalla, M.: Self-consistent formation of parallel electric fields in  
206 the auroral zone, Geophys. Res. Lett., 20, 475-478, 1993.
- 207 Stern, D.P.: One-dimensional models of quasi-neutral parallel electric fields, J. Geophys.  
208 Res., 86, 5839-5860, 1981.

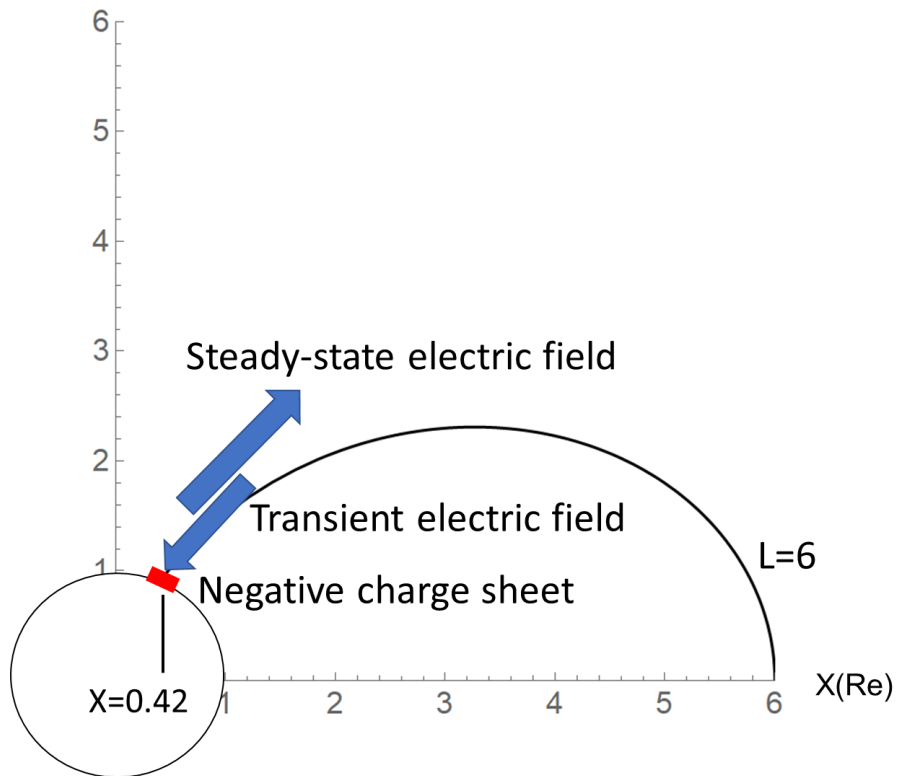


209

Figure 1

210 Altitude profiles of  $\sin^2 \alpha = B/B_R$  in dipole geometry of  $L=6$ .  $X (\text{Re})$  denotes equatorial  
 211 projection of the altitudes, from the ionosphere ( $X=0.42 \text{ Re}$ ) to 10,520 km above it ( $X=1.70$   
 212  $\text{Re}$ ).  $B_R$  represents field magnitudes at the ionosphere. Trapped particles filled area C. Loss  
 213 cone particles filled A. This curve can be given in the absence of the parallel electric fields.





214

215

Figure 2

216 Transient electric fields pointing into the ionosphere (downward) and steady-state electric  
 217 fields out of the ionosphere (upward) are discussed in the ionospheric injection scenario.

218 Negative charge sheet shown in red at polar ionosphere produced transient electric fields.

219 Steady-state electric field was initiated by the transient electric field via the Persson's

220 theorem (see text). Transient electric fields are shielded by the space charge deposited in

221 association with the onset of steady-state electric fields.

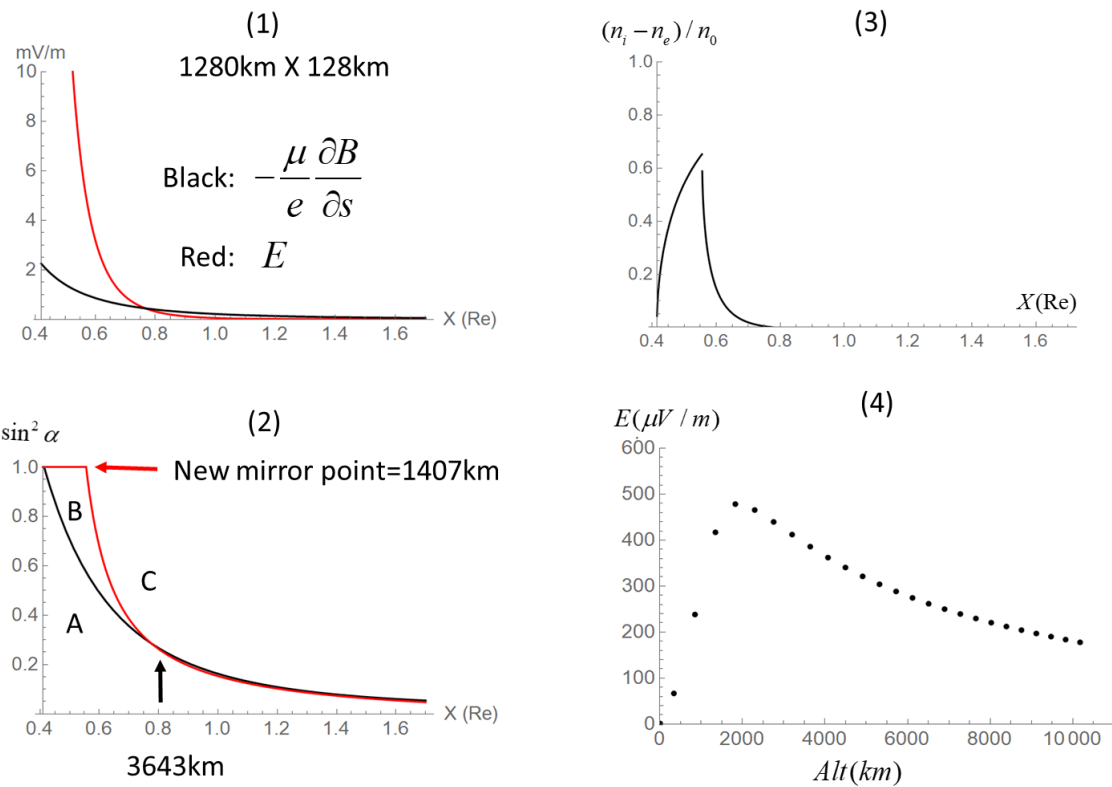


Figure 3

222 Negative charge sheet extending 1,280km in longitudes and 128km in latitudes are  
 223 generated in the polar ionosphere.

224

225 (1) Equatorial projection of altitude profiles of magnetic mirror force (black) and vertical  
 226 electric fields (red). X (Re) denotes equatorial projection of the altitudes, from the  
 227 ionosphere ( $X=0.42 \text{ Re}$ ) to 10,520 km above it ( $X=1.70 \text{ Re}$ ). It is assumed that  
 228  $\mu = 0.16 \text{ eV} / nT$ . Vertical electric fields exceed the magnetic mirror force below 3,643 km.

229 Note that amplitudes are presented in mV/m.

230

231 (2) Pitch-angle curve,  $\sin^2 \alpha = B/B_R$ , for electrons in the absence of the parallel electric  
 232 fields (black) and those modified by the vertical electric fields (red). Electrons when

233 affected by the vertical electric fields moved their mirror point to higher altitudes at 1,407  
234 km above the ionosphere. There are three regions in pitch-angle profiles, namely (A), (B),  
235 and (C) (see text).

236

237 (3) Difference of number density  $n_i - n_e$  normalized by  $n_0$ . Number densities of ions ( $n_i$ )  
238 and electrons ( $n_e$ ) are calculated by integrating Maxwellian distribution over velocity  
239 space. Plasma density in loss cone is empty (see text). The plot along L=6 started from  
240 the ionosphere ( $X=0.42$  Re) to 10,520km above it ( $X=1.70$  Re). Real density is given by  
241 multiplying  $n_0$ . Density gap at  $X=0.54$  Re is caused by discontinuous change of  $\sin^2 \alpha$ .

242

243 (4) Altitude profiles of steady-state electric fields  $E_{//}$  (upward,  $\mu V / m$ ) along field lines.  
244 Horizontal axis is altitudes in km of the field lines along L=6. Note that the ionosphere is  
245 at 0 km.

246

247

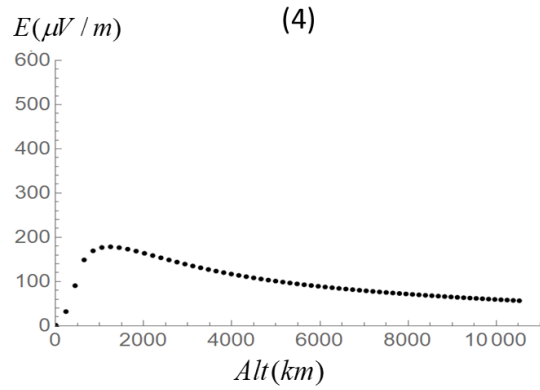
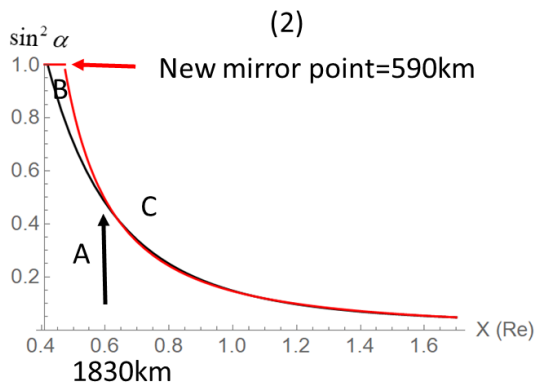
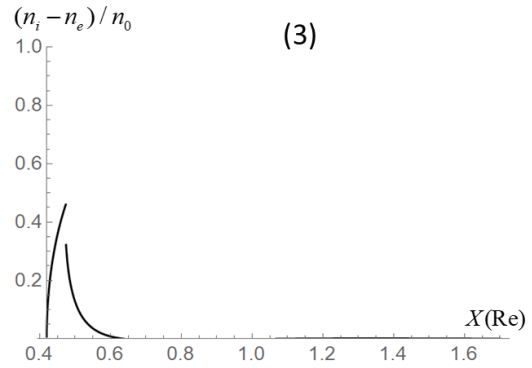
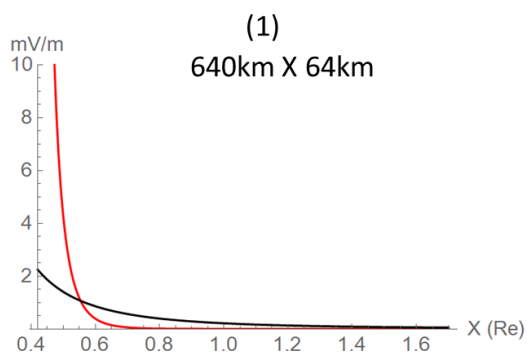


Figure 4

248 Same as Figure 3 but for half-sized negative charge sheet (640km in longitudes and 64km  
 249 in latitudes).  
 250